Supplementary Materials for

AI-designed AAV capsids deliver high-efficiency muscle gene transfer for low-dose therapy

Eva Petat *et al.*

Corresponding authors: Isabelle Richard, richard@genethon.fr, Ai Vu Hong, avuhong@genethon.fr

The PDF file includes:

Supplementary Figure 1 to Supplementary Figure 7

Table S1

Supplementary Figures

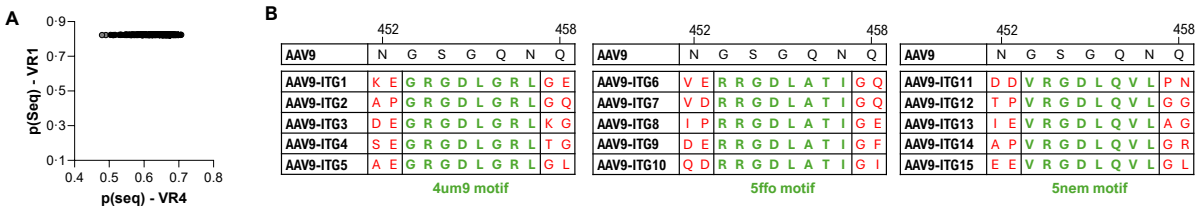

Supplementary Figure 1: Computational design of AAV9 capsids targeting αVβ6 integrin. **A**. Comparison of mean residue probabilities within VR1 and VR4 across all Rosetta-generated sequences. Optimization is restricted to VR4, consistent with the design strategy, while VR1 remains largely unchanged. **B**. Amino acid sequences of the VR4 loop for the 5 top capsid variants selected for each αVβ6-binding motif and subjected to experimental validation.

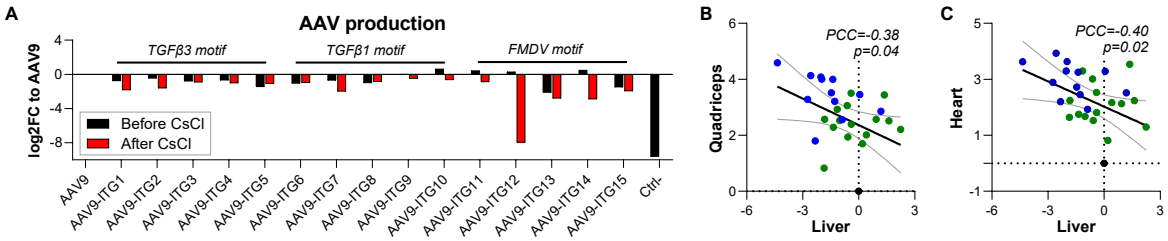

Supplementary Figure 2: Comparison of transduction efficiencies of designed AAV9 variants. **A**. Vector production yields of individual capsid variants in the barcoded library before and after CsCl-based purification. Negative control (Ctrl-): AAV9 capsid containing three premature stop codons in the cap ORF, abolishing expression of VP1, VP2 and VP3. **B-C**. Scatter plots showing the inverse correlation between transduction efficiency in liver and quadriceps muscle (**B**) or liver and heart (**C**) for AAV9-ITG1–9 capsid variants. PCC: Pearson correlation coefficient. Data are presented as $\log_2$ fold-change (log2FC) relative to AAV9. Correlation analysis in **B-C** was performed using Pearson's method.

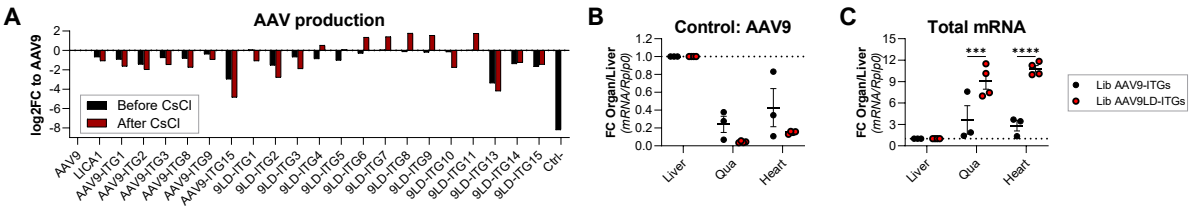

Supplementary Figure 3: Barcoded library design reshapes tissue distribution toward skeletal and cardiac muscle. **A**. Vector production yields of individual capsid variants in the barcoded library before and after CsCl-based purification. Negative control (Ctrl-): AAV9 capsid containing three premature stop codons in the cap ORF, abolishing expression of VP1, VP2 and VP3. **B-C**. Comparison of transgene mRNA levels in liver, skeletal muscle and heart following systemic administration of the AAV9-ITG and AAV9LD-ITG libraries. Data are shown for AAV9 alone (**B**) or for all variants within each library (**C**), expressed as $\log_2$ ratios of indicated tissues relative to liver. Whereas parental AAV9 shows reproducibly higher transgene expression in liver, consistent with its intrinsic liver tropism, variants within the AAV9LD-ITG library display a shifted distribution with higher transgene expression in skeletal muscle and heart compared with liver, and significantly higher muscle and cardiac expression than the AAV9-ITG library. This redistribution improved the identification of myotropic capsid variants. Data are presented as mean ± SEM. Statistical analyses were performed using one-way ANOVA followed by FDR correction. *p < 0.05; **p < 0.01; ***p < 0.001; ****p < 0.0001; ns not significant.

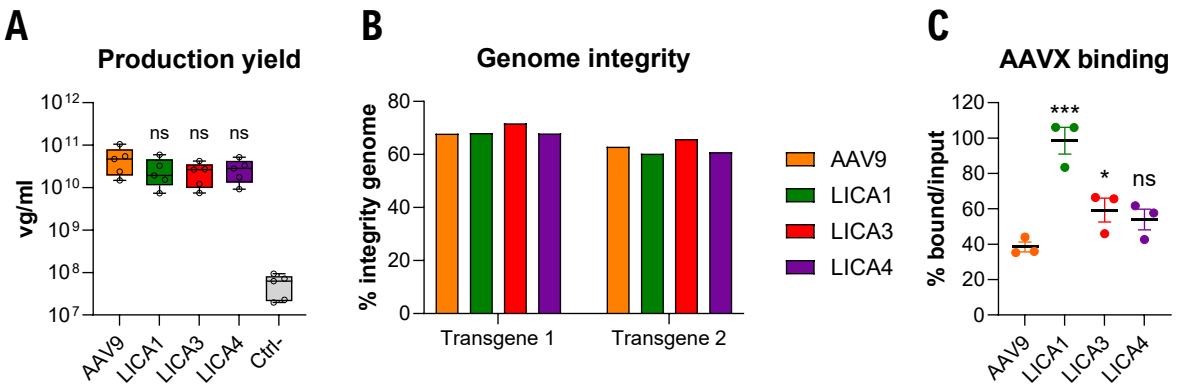

Supplementary Figure 4: LICA3 and LICA4 exhibit improved manufacturability. Vector manufacturability was evaluated by production yield (**A**, 5 biological replicates), integrity of packaged vector genomes assessed by droplet digital PCR using two independent transgenes (**B**), and capsid binding efficiency to AAVX affinity resin (**C**, 3 biological replicates). Data are presented as mean ± SEM. Statistical analyses were performed using one-way ANOVA followed by FDR correction. *p < 0.05; **p < 0.01; ***p < 0.001; ****p < 0.0001; ns not significant.

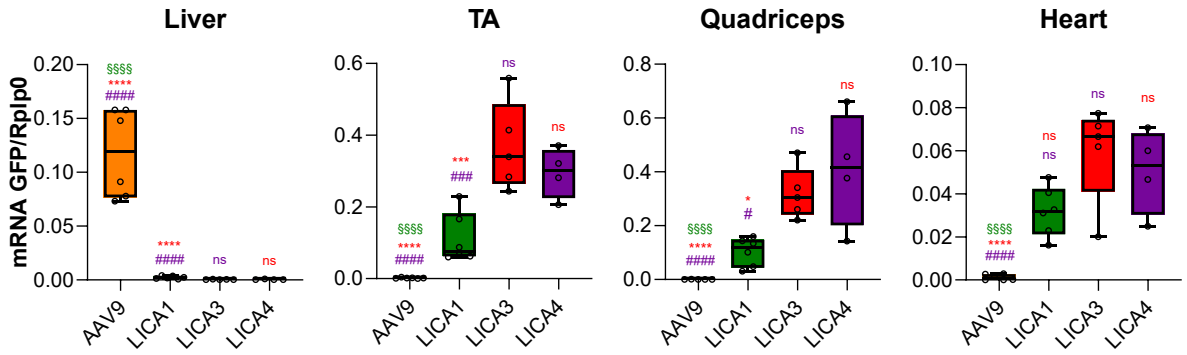

Supplementary Figure 5: LICA3 and LICA4 showed improved transgene expression (mRNA level) in skeletal and cardiac muscles and strongly liver-detargeted at 3dpi, relative to AAV9 and LICA1. Data are presented as mean ± SEM. Statistical analyses were performed using one-way ANOVA followed by FDR correction. *p < 0.05; **p < 0.01; ***p < 0.001; ****p < 0.0001; ns not significant.

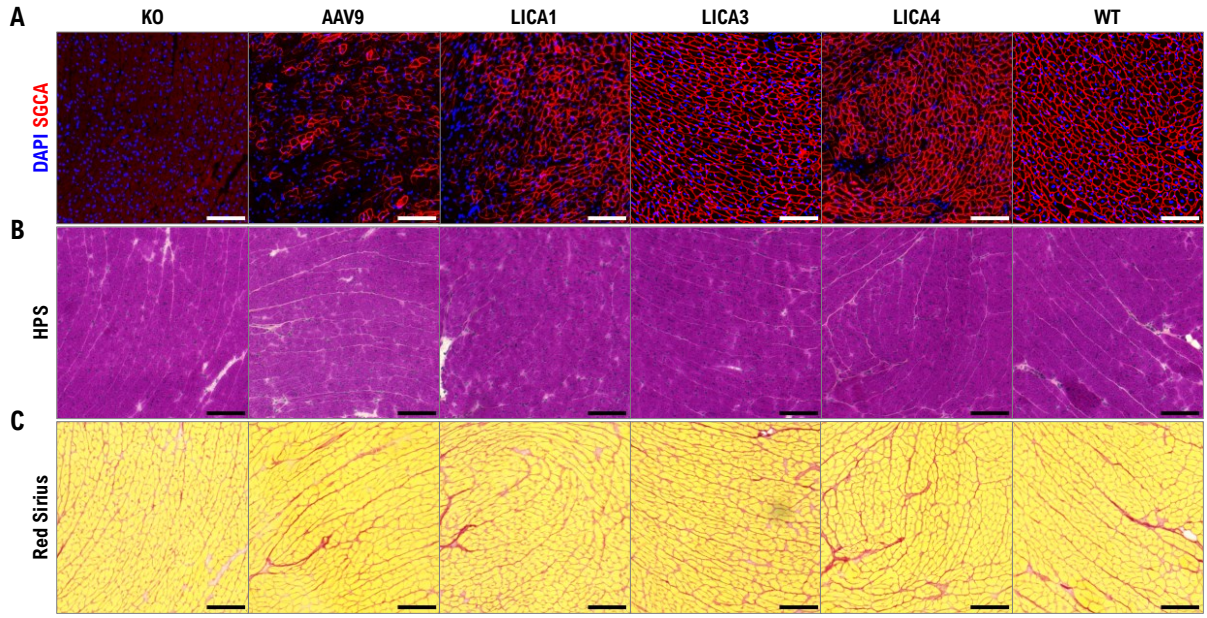

Supplementary Figure 6: Cardiac transduction and histopathological evaluation following low-dose systemic gene therapy in an LGMDR3 mouse model. Representative cardiac sections stained for SGCA (**A**), haematoxylin–phloxine–saffron (HPS, **B**) and Sirius Red (**C**) following treatment with the indicated AAV capsids (Scale bar: 100µm). All three LICA variants demonstrate a significantly higher proportion of SGCA-positive cardiomyocytes compared with AAV9. At this dose, LICA3 and LICA4 achieve near-complete cardiomyocyte transduction. SGCA localization is restricted to sarcolemma, and no histopathological abnormalities or evidence of cardiac toxicity are observed.

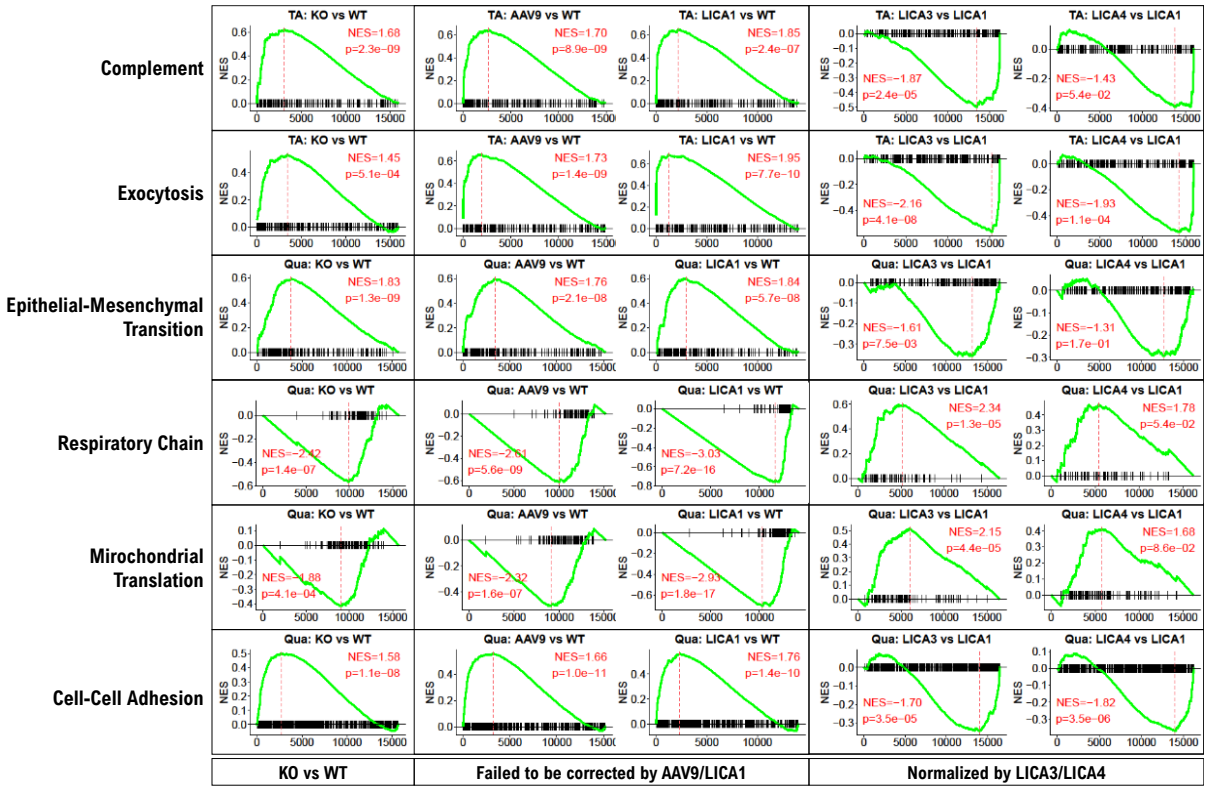

Supplementary Figure 7: Transcriptomic normalization by LICA3 and/or LICA4. Gene set enrichment analysis of pathways dysregulated in SGCA-KO muscle and insufficiently restored by AAV9 or LICA1 treatment but further normalized by LICA3 and/or LICA4.

Supplementary Tables

Table S1: Table of primers used in qPCR and ddPCR analysis.

Primer	Forward (5'-3')	Reverse (5'-3')	Probe (if Taqman)
Rplp0	CTCCAAGCAGATGCAGCAGA	ATAGCCTTGCGCATCATGGT	CCGTGGTGCTGATGGGCAAGAA
ITR	GGAACCCCTAGTGATGGAGTT	CGGCCTCAGTGAGCGA	CACTCCCTCTCTGCGCGCTCG
SGCA	TCTGGATGTCGGAGGTAGCC	TGCTGGCCTATGTCATGTGC	CGGGAGGGAAGGCTGAAGAGAGACC
GFP	AGTCCGCCCTGAGCAAAGA	GCGGTCACGAACTCCAGC	CAACGAGAAGCGCGATCACATGGTC
CMV	CATCAATGGGCGTGGATAGC	GGAGTTGTTACGACATTTTGGAAA	ATTTCCAAGTCTCCACCC
bGH_pA	TCTAGTTGCCAGCCATCTGTTGT	TGGGAGTGGCACCTTCCA	TCCCCCGTGCCTTCCTTGACC
HBB2_pA	CCAGGCGAGGAGAAACCA	CTTGACTCCACTCAGTTCTCTTGCT	CTCGCCGTAAAACATGGAAGGAACACTTC
mCherry-BC001	TGGACATCACCTCCCACAAC	GTATATACAACGAGTCTGTCTCG	
mCherry-BC002	TGGACATCACCTCCCACAAC	GTCGGTTTAAATCTCTAGTCTCG	
mCherry-BC003	TGGACATCACCTCCCACAAC	GTCCATCCGCTGTCACG	
mCherry-BC004	TGGACATCACCTCCCACAAC	TGACCCTGACCGCCCAG	
mCherry-BC005	TGGACATCACCTCCCACAAC	GTCTCGAAGGACGGCAAG	
mCherry-BC006	TGGACATCACCTCCCACAAC	TGGCCCGTCCGCTGAA	
mCherry-BC007	TGGACATCACCTCCCACAAC	GGTACTGTAAAGAGCGGACTGAC	
mCherry-BC008	TGGACATCACCTCCCACAAC	GTCGACCAGGATCTTAAGTCTCG	
mCherry-BC009	TGGACATCACCTCCCACAAC	GTCGTTGCCCATGTTGAGT	
mCherry-BC010	TGGACATCACCTCCCACAAC	GTTGGGCGTCGATCAAGG	
mCherry-BC011	TGGACATCACCTCCCACAAC	GTAGATTGAATAGCGTAGTCTCG	
mCherry-BC012	TGGACATCACCTCCCACAAC	GTATCCGCCAGAAGCACG	
mCherry-BC013	TGGACATCACCTCCCACAAC	TGGCGACCGACAGCCG	
mCherry-BC014	TGGACATCACCTCCCACAAC	GTTCAGTAACGTACGATGTCTCG	
mCherry-BC015	TGGACATCACCTCCCACAAC	GTCTATGCTTTCGAATCGTCTCG	
mCherry-BC016	TGGACATCACCTCCCACAAC	GTTCCGGACCCGATACG	
mCherry-BC017	TGGACATCACCTCCCACAAC	GTCCACAAACCCAACCAGTC	
mCherry-BC018	TGGACATCACCTCCCACAAC	GTGTACCGTTACAACGAGTCTC	
mCherry-BC019	TGGACATCACCTCCCACAAC	GTGGCAACCCAACGTTAGT	
mCherry-BC020	TGGACATCACCTCCCACAAC	GTGCCCTTCTAGTGGTCG	
mCherry-BC021	TGGACATCACCTCCCACAAC	GTCCTCCTCGACTTCTGG	
mCherry-BC022	TGGACATCACCTCCCACAAC	TAGGAACTCGTCGGCTGT	
mCherry-BC023	TGGACATCACCTCCCACAAC	GTGAGCTGACACCAGATGTC	
mCherry-BC024	TGGACATCACCTCCCACAAC	TCGTACCGCTGTTGAGGTC	
mCherry-BC025	TGGACATCACCTCCCACAAC	TGCATGGTGGTAGTCTGTCT	
mCherry-BC026	TGGACATCACCTCCCACAAC	TGTACACTGCATTGGCGTC	
mCherry-BC027	TGGACATCACCTCCCACAAC	TCCTCAGTGCACCTCTGTC	
mCherry-BC028	TGGACATCACCTCCCACAAC	GTGGCAGTGTTCCTGTTGTC	
mCherry-BC029	TGGACATCACCTCCCACAAC	GTGCGAGAGTCCTCTAGGTC	
mCherry-BC030	TGGACATCACCTCCCACAAC	GTGTACTCGGATAAGCTGTCTC	
mCherry-BC031	TGGACATCACCTCCCACAAC	GTCTACTCAGCGACATTGTCTC	
mCherry-BC032	TGGACATCACCTCCCACAAC	GTAGAGCTAGAGTCAAGGTCTCG	